Extracellular vesicles carrying surface-anchored adiponectin prevent obesity-related metabolic complications by enhancing insulin sensitivity

Alexia Blandin[3,#], Josy Froger[1,2,#], Margot Voisin[1,2], Maëlle Lachat[3], Grégory Hilairet[2], Katarzyna Polak[3], Julie Magusto[1,2], Lisa Meslier[1,2], Mikaël Croyal[1,4], Mathilde Gourdel[4], Quentin Massiquot[2], Julien Chaigneau[5], Maxime Carpentier[1], Lionel Fizanne[5], Xavier Prieur[1], Cédric Le May[1], Jérôme Boursier[5], Bertrand Cariou[1], Robert Mamoun[3], Bernadette Trentin[3] and Soazig Le Lay[1,2,*]

[1]Nantes Université, CHU Nantes, CNRS, INSERM, l'institut du thorax, F-44000 Nantes, France.

[2]Université Angers, *SFR* ICAT, 49000 Angers, France

[3]Ciloa, 356 rue Maurice Béjart, 34080 Montpellier, France

[4]Nantes Université, CHU Nantes, Inserm, CNRS, SFR Santé, Inserm UMS 016, CNRS UMS 3556, Nantes, France

[5]HIFIH, CHU Angers, Université Angers, *SFR* ICAT, 49000 Angers, France

[#]These authors equally contributed to this work

***Corresponding author: Soazig LE LAY**

L'unité de recherche de l'institut du thorax

Inserm UMR1087/CNRS UMR6291, IRS-UN – 8 quai Moncousu – BP 70721 44007 Nantes Cedex 1

e-mail: soazig.lelay@inserm.fr, Tel: +33-244-688-413

Keywords

Extracellular vesicles, exosomes, obesity, type 2 diabetes, MASLD, MASH, biotherapy, bioengineering, EV-based therapy

4 Main Figures, 1 Supplementary Table**,** 3 Supplementary Figures

Total words (Introduction, Methods, Results and Discussion) : **3579**

References : 27

Abbreviations:

ACC, acetyl-CoA carboxylase; ACLY, ATP citrate lyase; AdipoQ, adiponectin gene; Col1A1, collagen type I alpha 1; ELOVL6, elongation of very long chain fatty acids protein 6; F4/80, EGF-like module-containing mucin-like hormone receptor-like 1 (macrophage marker); FAS, fatty acid synthase; IL-1β, interleukin-1 beta; IL-6, interleukin-6; MCP1, monocyte chemoattractant protein 1; PDK4, pyruvate dehydrogenase kinase 4; PGC1α, peroxisome proliferator-activated receptor gamma coactivator 1-alpha; PLIN1, perilipin 1; PLIN2, perilipin 2; PPARγ2, peroxisome proliferator-activated receptor gamma isoform 2; TGF-β1, transforming growth factor beta 1.

Abstract (197 words)

Adiponectin (Adpn) is a potent insulin-sensitizing adipokine with therapeutic promise for type 2 diabetes (T2D) and metabolic dysfunction-associated steatohepatitis (MASH). Its clinical use remains limited due to difficulties in producing stable, bioactive high–molecular weight forms. We previously demonstrated that adipose tissue-derived extracellular vesicles (EVs) naturally carry oligomeric Adpn on their surface, enhancing its stability and activity. Here, we engineered EVs displaying Adpn either anchored to the membrane ($EV^{PP\text{-}Adpn}$) or soluble (EV^{Adpn}), alongside control EVs lacking Adpn (EV^{CTL}), and evaluated their effects in a diet-induced obesity mouse model.

Mice received twice a week intraperitoneal injections of EVs or vehicle for six weeks. Only $EV^{PP\text{-}Adpn}$ significantly improved insulin sensitivity and reduced weight gain. Mechanistically, $EV^{PP\text{-}Adpn}$ enhanced adipocyte lipid storage through upregulation of insulin-responsive lipogenic genes and reduced hepatic steatosis, inflammation and fibrosis markers. It also activated AKT and AMPK pathways in liver and skeletal muscle, consistent with adiponectin signaling. In addition, $EV^{PP\text{-}Adpn}$ lowered circulating ceramides, lipids molecules promoting insulin resistance, in agreement with ceramidase activity induced by adiponectin receptor (AdipoR) signaling.

Our results demonstrate that surface-anchored Adpn EVs restore tissue-specific insulin signaling and ameliorate metabolic dysfunctions, highlighting their potential as a novel biotherapeutic strategy for T2D and MASH.

Introduction

The increasing global prevalence of type 2 diabetes (T2D) and its associated cardiometabolic complications underscores an urgent need for innovative therapeutic strategies, particularly given the limited availability of effective insulin-sensitizing molecules.

Among potential targets, adiponectin (Adpn) has emerged as a promising candidate due to its insulin-sensitizing, anti-inflammatory, and cardioprotective properties. Adpn, an adipokine, also known as adipocyte complement-related protein of 30 kDa (Acrp30), is specifically secreted by adipocytes [1]. Adpn abundantly circulates in blood in multimeric forms [2], and its plasma concentrations is decreased in patients with obesity and T2D [3]. Mechanistically, multimeric forms of Adpn exerts their effects through the activation of its receptors, AdipoR1 and AdipoR2, which are widely expressed in metabolic tissues [4]. These receptors mediate downstream signaling pathways such as AMP-activated protein kinase (AMPK) and peroxisome proliferator-activated receptor-α (PPARα), promoting glucose uptake, fatty acid oxidation, and anti-inflammatory responses [5]. However, the clinical translation of recombinant Adpn-based therapies has been hindered by significant challenges, especially the production of stable high molecular weight (HMW) Adpn oligomers.

We recently demonstrated that extracellular vesicles (EVs) derived from adipocytes are naturally coated with Adpn oligomers and act as natural cargos of Adpn accounting for 20% of the Adpn circulating pool [6]. Our results also demonstrated enhanced stability of EV-associated Adpn oligomers in the bloodstream compared to free Adpn as well as maintenance of Adpn-associated EVs' insulin-sensitizing effects [6]. EVs are lipid bilayer-enclosed structures secreted by various cell types, and they serve as carriers for bioactive molecules, including proteins, lipids, and nucleic acids [7]. EVs display natural abilities to cross biological barriers and interact with cells, modulating target cell responses and displaying immunomodulatory and regenerative activities [8]. Thus, EVs have recently emerged as promising drug delivery nano-vehicles due to their high bioavailability, excellent biocompatibility, and minimal immunogenicity, highlighting their potential as innovative therapeutic carriers [9].

This study aims to harness EVs as delivery systems for bioactive Adpn oligomers to treat metabolic disorders. To this goal, we mastered the production of customized EVs presenting oligomerized forms of Adpn at their surface and assess their therapeutic potential in mitigating insulin resistance and metabolic dysfunctions of high-fat diet fed mice. Treatment of these mice with EVs presenting Adpn at their surface enhances adipocyte lipid storage through insulin-regulated lipogenesis and lipid storage gene induction, while improving Metabolic dysfunction-Associated SteatoHepatitis (MASH) lesions (steatosis, inflammation, fibrosis) by restoring hepatic insulin sensitivity. Altogether, our results demonstrate the insulin-sensitizing potential

96 of surface Adpn-exposing EVs, paving the way for an innovative biotherapy for managing T2D
97 and MASH.
98
99 **Methods**
100 ***Animal experiments***
101 Male and female C57BL/6J (B6) mice (10 weeks old) were fed a high-fat diet (HFD; 61% kcal
102 from fat, 20% protein, 20% carbohydrate; D12492, Safe Diets) *ad libitum* for 6 weeks. Mice
103 were housed under standard conditions (12 h light/12 h dark cycle) with *ad libitum* access to
104 food and water. During the HFD period, mice received biweekly intraperitoneal (i.p.) injections
105 of EVs, resuspended in 100 µL sterile 0.9% NaCl. Control animals received an equivalent
106 volume of PBS in 0.9% NaCl as vehicle. All procedures were approved by the French Ministry
107 of Research and the local ethics committee (CEEA - 006) and complied with EU Directive
108 2010/63/EU. At sacrifice, tissues were collected from either random-fed mice or after a 4 h fast
109 followed by insulin injection. At the end of the experiment, body weight and the weights of
110 organs/tissues, including liver, visceral white adipose tissue (VAT), subcutaneous white
111 adipose tissue (SAT), interscapular brown adipose tissue (BAT), pancreas, spleen and
112 quadriceps (representative of skeletal muscle) were recorded. Adiposity (%) was calculated as
113 the sum of VAT and SAT weights divided by total body weight. Samples were fixed in 10%
114 formalin for histological analysis or snap-frozen in liquid nitrogen and stored at –80 °C for
115 molecular analyses.
116
117 ***Hepatic Lipid Quantification***
118 Hepatic lipids were extracted from snap-frozen liver samples using a modified Bligh and Dyer
119 method[10]. Hepatic triglycerides (TG) were quantified using enzymatic kits (Roche Diagnostics)
120 and expressed relative to liver weight (µg TG per g of liver tissue).
121
122 ***Plasma FGF21 Measurement***
123 Circulating FGF21 concentrations was measured using commercial ELISA kits designed for
124 mouse measurments (R&D systems) from plasma samples according to the manufacturer's
125 protocol.
126
127 ***Metabolic Testing and Insulin Signaling Assessment***
128 Glucose (tolerance test (GTT) and insulin (tolerance test (ITT) were conducted during the fifth
129 week of EV injections. Mice were fasted for 4 hours prior to testing. For GTT, glucose (1.25
130 g/kg body weight) was administered intraperitoneally (i.p.) at time 0. For ITT, mice were
131 injected i.p. with 0.75 IU/kg body weight human insulin (Humulin, Lilly) at time 0. Blood glucose
132 was measured from tail vein samples at 0, 15, 30, 45, 60, 90, and 120 minutes using

133 glucometer strips (Accu-Chek Guide). Plasma insulin concentrations were determined using
134 commercial mouse ELISA kits (Crystal Chem) from serum samples collected during the GTT
135 on heparin-coated microvettes (Sarstedt) following the manufacturer's instructions
136 To evaluate insulin signaling in target tissues, mice were fasted for 4 hours and injected i.p.
137 with human insulin (3 IU/kg; Humulin, Lilly). Tissues were collected 15 minutes post-injection
138 for analysis of insulin response.

139 ***Western blot***

140 Insulin and AMPK signaling were assessed in mouse tissues collected 15 minutes after i.p.
141 insulin injection. VAT, SAT, and skeletal muscle (quadriceps) were harvested at this time point.
142 Tissue homogenization was performed on 20mg of snap-frozen liver or muscle tissue and 100
143 mg of snap-frozen VAT using CK14 soft tissue beads and the Precellys homogenizer,
144 according to the manufacturer's instructions. Protein lysates (15 µg) were subjected to SDS–
145 PAGE and Western blotting, as previously described[11]. The following primary antibodies were
146 used: phospho-Akt (Ser473, #4060), total Akt (pan, #4691), phospho-AMPKα (Thr172, #2535)
147 and total AMPKα (#2532) (Cell Signaling Technology), GAPDH (#ABC-AC002-100, ABclonal),
148 and β-actin (#A5316, Sigma-Aldrich). IRDye-conjugated secondary antibodies (LI-COR
149 Biosciences) were used, and signals were detected using an Odyssey CLx imaging system
150 (LI-COR). Quantification was performed using Image Studio software. Representative blots
151 per protein shown include samples from at least three independent animals per group.
152

153 ***Histology and tissue staining***

154 Adipose and liver tissues were fixed in 10% PBS-buffered formalin for at least 24 hours,
155 paraffin-embedded, and sectioned at 5 µm. After deparaffinization and rehydration with specific
156 commercial solutions (Impath), sections were stained with with hematoxylin and eosin (HE) for
157 morphology and picrosirius red (PS) to assess fibrosis. Adipocyte diameter (VAT, SAT),
158 steatosis and fibrosis areas (liver) were quantified using dedicated ImageJ plugins.
159

160 ***RNA Extraction and qPCR***

161 RNA was extracted from liquid nitrogen–frozen tissues. For VAT, RNA was isolated using
162 QIAzol and purified with the RNeasy Microkit (Qiagen), including DNase I treatment. Liver and
163 muscle RNA were extracted using the Maxwell® RSC simplyRNA Tissue Kit and instrument
164 (Promega). RNA quantity and purity were assessed via NanoDrop ND-2000 (Thermo Fisher).
165 cDNA was synthesized from 1 µg RNA using SuperScript™ II (Invitrogen) and random
166 hexamers, then purified with the Qiaquick PCR kit (Qiagen). qPCR was performed with 3 ng
167 cDNA, Maxima™ SYBR Green Master Mix (Thermo Fisher), and 0.3 µM primers using a CFX
168 Opus 384 system (Bio-Rad). Cycling conditions were 95°C for 10 min, then 40 cycles of 95°C

169 for 15 s and 60°C for 30 s. Specificity was confirmed by melting curve analysis. Gene
170 expression was calculated via the $2^{-\Delta\Delta Cq}$ method, normalized to 18S and 36B4, and analyzed
171 with CFX Maestro (Bio-Rad). Primer sequences are available upon request.
172
173 ***Ceramide analysis by mass spectrometry***
174 Ceramides were quantified from 10 µL of plasma using targeted lipid liquid chromatography–
175 tandem mass spectrometry (LC-MS/MS), as previously described [11].
176
177 ***Quantification and Statistical Analysis***
178 Data were analyzed with GraphPad Prism and presented as dot plots of independent
179 experiments. Statistical tests used are specified in figure legends. Significance was set at $p \leq$
180 0.05, indicated as *$p \leq 0.05$, **$p \leq 0.01$, ***$p \leq 0.005$, and ****$p \leq 0.001$.
181
182
183
184
185

186 **Results**

187

188 ***Generation and characterization of bioengineered EVs carrying Adpn.***

189 To exploit the therapeutic potential of Adpn-associated EVs, we engineered EVs carrying
190 native forms of Adpn according to a patented technology [12]. To this end, we used two chimeric
191 gene constructs encoding either wild-type Adpn or Adpn anchored to the EV surface via its N-
192 terminus, achieved by fusing the Adpn gene to a transmembrane domain and a pilot peptide
193 (PP-Adpn) that directs it towards the EV secretion pathway (Figure S1A). Bioengineered EVs
194 were isolated from the supernatants of HEK 293T cell lines stably transfected with Adpn
195 (EV^{Adpn}) or with PP-Adpn ($EV^{PP\text{-}Adpn}$), using a controlled purification process combining
196 tangential flow filtration and chromatography. In parallel, control EVs (EV^{CTL}) were produced
197 from the supernatants of non-transfected HEK 293T cells. All EV preparations showed
198 enrichment of the EV markers Alix and syntenin-1, as demonstrated by Wlestern blot (Figure
199 S1B), and of CD81, as shown by ELISA (Figure S1C). Nano-flow cytometry analysis indicated
200 that the size distribution of both control EVs and bioengineered EVs was within the expected
201 range for EVs (50-120 nm) (Figure S1D), with no significant differences in EV median size
202 (~70-90 nm) or concentration (~10^{10} particles/mL) among preparations (Figure S1E-F).
203 Quantification of Adpn content per EV confirmed successful and consistent loading across
204 bioengineered EV batches, while Adpn was undetectable in control EVs (Figure S1G). Western
205 blot analysis of EV^{Adpn} and $EV^{PP\text{-}Adpn}$ confirmed the presence of Adpn, with a molecular weight
206 consistent with the designed construct (Figure S1H). EV-associated Adpn was present in its
207 high-molecular-weight proteo-oligomeric forms in both bioengineered EVs, which are
208 recognized as the metabolically active forms (Figure S1I).

209

210 ***Dose-dependent metabolic effects of bioengineered EVs***

211 As part of our investigation into the metabolic effects of bioengineered EVs carrying Adpn, we
212 first sought to determine an effective and physiologically relevant dosing strategy. EV^{Adpn}, $EV^{PP\text{-}}$
213 ^{Adpn} and EV^{CTL} were administered by IP injections twice a week over a 6-week period to 10-
214 week-old mice fed a high-fat diet (HFD). Three doses of EV-associated Adpn (0.5 ng, 2.5 ng,
215 and 25 ng) were tested, with dosing standardized to the quantified Adpn content of each EV
216 preparation (Figure S2A-B). The lowest dose (0.5 ng) matched the Adpn amount found in 5 µg
217 of VAT-derived EVs previously shown to enhance insulin sensitivity[6]. The amount of EV^{CTL},
218 devoid of any Adpn, was matched to the highest particle number used among EV^{Adpn} and $EV^{PP\text{-}}$
219 ^{Adpn} to control for potential particle-related effects (Figure S2B). A PBS-injected group served
220 as vehicle control to distinguish Adpn-associated EV specific effects.

221 The highest dose (25 ng) of EV^{CTL} and EV^{Adpn} (1.45×10^8 EVs/injection; Figure S2B) increased
222 weight gain after 6 weeks of HFD compared to the lowest dose (0.5 ng; Figure S2C-D;F-G),

223 and was associated with increased BAT weight for EV^{CTL} (Figure S2K) and higher spleen
224 weight for EV^{Adpn} (Figure S2N). Likewise, the lowest dose (0.5 ng) of $EV^{PP\text{-}Adpn}$ (1.0×10^7 EVs)
225 significantly increased weight gain versus vehicle (Figure S2E;H), along with elevated
226 subcutaneous AT (SAT) weight (Figure S2J) and higher glycemia in both fed and fasted states
227 (Figure S2O-P). In contrast, 25 ng of $EV^{PP\text{-}Adpn}$ (5.0×10^8 EVs) significantly reduced both weight
228 gain and SAT mass compared to its 0.5 ng dose (Figure S2E;H;J), despite involving more
229 particles (Figure S2B). These findings suggest that higher EV concentrations may worsen
230 metabolic outcomes under HFD, unless EVs are surface-coated with Adpn, as illustrated with
231 high-dose $EV^{PP\text{-}Adpn}$. Based on these observations, the highest dose (25 ng) was selected for
232 subsequent experiments to enable comprehensive metabolic phenotyping of bioengineered
233 EVs and their therapeutic potential.
234
235 ***Surface Adpn-anchored EVs ($EV^{PP\text{-}Adpn}$) improve insulin sensitivity and glucose***
236 ***tolerance***
237 Male and female HFD-fed mice were thus treated with EV^{CTL}, EV^{Adpn} or $EV^{PP\text{-}Adpn}$ (at 25 ng
238 Adpn-equivalent doses, or equivalent particle numbers for EV^{CTL}), or with vehicle (PBS), to
239 assess their metabolic effects. No significant differences in body weight over time (Figure 1A),
240 weight gain (Figure 1B) or adiposity at sacrifice (Figure 1C) were observed between groups,
241 regardless of sex. Similarly, no significant differences in individual tissue weights (including AT
242 depots, liver, pancreas, spleen and muscle) were detected between groups at sacrifice,
243 indicating the absence of hepatomegaly or splenomegaly and supporting the lack of EV-
244 induced organotoxicity (Figure S3A-G). In addition, serum biochemistry analyses (Table S1)
245 revealed no signs of hepatic or renal toxicity, further supporting the safety of repeated EV
246 injections. Random-fed glycemia, monitored throughout the experiment, remained stable in
247 both females and males (Figure 1D), as did fasting glycemia, measured at the end of the
248 protocol (Figure 1E). Insulin tolerance tests (ITT) demonstrated a significant improvement in
249 insulin sensitivity exclusively in $EV^{PP\text{-}Adpn}$ treated mice of both sexes, as indicated by increased
250 area over the curve (AOC) (Figure 1F). Similarly, intraperitoneal glucose tolerance tests (IP-
251 GTT) showed improved glucose tolerance in males treated with $EV^{PP\text{-}Adpn}$, while in females,
252 both EV^{Adpn} and $EV^{PP\text{-}Adpn}$ enhanced glucose tolerance (Figure 1G). Glucose intolerance
253 induced by HFD is often associated with impaired insulin secretion. In the $EV^{PP\text{-}Adpn}$-treated
254 group, the improvement in glucose tolerance was accompanied by the restoration of the 15-
255 minute insulin peak following glucose load (T15 vs. T0), which was absent in all other groups
256 (Figure 1H). No such induction was detected in any group of females (Figure 1H). These
257 improvements occurred without detectable changes in pancreatic β-cell mass or size, as
258 indicated by comparable insulin immunostaining across groups on pancreatic sections (Figure
259 S3K-N).

260

261 ***EV$^{PP\text{-}Adpn}$ promote healthy adipose tissue expansion***

262 Although total AT mass remained unchanged across groups at the end of treatment (Figure
263 1C, Figure S3A-C), histological analysis of VAT revealed a significant shift in adipocyte size
264 distribution toward larger diameters in both EV^{Adpn} and EV$^{PP\text{-}Adpn}$ treated mice, reflecting an
265 increase in average adipocyte size (Figure 2A-C). This effect was specific to VAT and was not
266 observed in SAT (Figure S3H-J). Importantly, only EV$^{PP\text{-}Adpn}$ treatment resulted in a coordinated
267 upregulation of mRNA levels for key adipocyte markers such as PPARγ2, PLIN1, and AdipoQ
268 (Figure 2D), as well as insulin-regulated lipogenic enzymes gene expression including
269 ELOVL6, FAS, ACC and ACLY (Figure 2E). No significant changes were detected in the
270 expression of inflammatory genes (IL1β, MCP1, F4/80, IL6) (Figure 2F). Of note, circulating
271 NEFA levels were unchanged across groups (Table S1), indicating that basal lipolysis is not
272 altered by any EV treatments. These histological and molecular changes indicate that EV$^{PP\text{-}}$
273 ^{Adpn} promote insulin-sensitive AT expansion, consistent with the known effects of Adpn on these
274 pathways, which likely support more efficient fat storage and healthier adipose tissue
275 remodeling.

276

277 ***EV$^{PP\text{-}Adpn}$ alleviate liver steatosis and MASH-related gene expression***

278 Liver histology revealed a marked reduction in steatosis in EV$^{PP\text{-}Adpn}$–treated animals (Figure
279 3A–B), further supported by a significant decrease in hepatic triglyceride content (Figure 3D)
280 and reduced protein expression of PPARγ2 (Figure 3E-F). In line with these findings, serum
281 biochemistry analyses revealed significant improved liver enzyme profiles (ALAT, ASAT) in
282 both EV^{Adpn} and EV$^{PP\text{-}Adpn}$ treated groups (Table S1), supporting the beneficial hepatic effects
283 observed histologically. Although fibrosis area remained unchanged across liver sections
284 (Figure 3C), consistent with the limited fibrotic response in HFD-fed mouse models, we
285 observed a significant downregulation of MASLD-related genes in the EV$^{PP\text{-}Adpn}$ group. These
286 included the lipid droplet marker PLIN2, pro-inflammatory genes (IL1β, MCP1, F4/80), and
287 fibrotic markers (TGFβ1, Col1A1) (Figure 3G), indicating improved lipid handling and
288 attenuated inflammatory and fibrotic signaling.

289 Analysis of hepatic metabolic gene expression showed no major changes in lipogenic (FAS,
290 ACC) or oxidative (PDK4, PGC1α) genes (Figure 3H). Phosphoenolpyruvate Carboxykinase
291 (PEPCK) is a gluconeogenic enzyme normally downregulated by insulin, but this repression is
292 lost in HFD-fed mice[13]. EV$^{PP\text{-}Adpn}$ treatment restored this repression, as shown by a significant
293 reduction in PEPCK mRNA expression, with a similar trend observed for glucose-6-
294 phosphatase **(**G6Pase) (Figure 3H).

295 Circulating FGF21, a hepatokine elevated in response to liver fat accumulation and metabolic
296 stress, was drastically reduced in EV$^{PP\text{-}Adpn}$ treated mice (Figure 3I). Previous reports have

297 shown that increased FGF21 reflects a compensatory but dysregulated response to hepatic
298 lipid overload and impaired metabolic signaling in MASLD [14,15]. Therefore, the reduction of
299 FGF21 following $EV^{PP\text{-}Adpn}$ treatment likely indicates improved hepatic lipid metabolism and
300 restored metabolic homeostasis.
301 These findings suggest that $EV^{PP\text{-}Adpn}$ selectively restores hepatic insulin responsiveness at the
302 transcriptional level and alleviates key features of MASH, including steatosis, inflammation,
303 and fibrotic gene expression, thereby highlighting its therapeutic potential in MASLD.
304
305 ***$EV^{PP\text{-}Adpn}$ promotes adiponectin-dependent insulin signaling and ceramide clearance***
306 To further investigate the insulin-sensitizing effects of bioengineered EVs displaying surface-
307 anchored adiponectin ($EV^{PP\text{-}Adpn}$), we evaluated the activation of key adiponectin-responsive
308 signaling pathways in VAT, liver, and skeletal muscle following acute insulin stimulation (3 U,
309 15 min). Western blot analyses revealed an increased insulin-stimulated phosphorylation of
310 AKT (Ser473) in all examined tissues of $EV^{PP\text{-}Adpn}$ treated mice compared to EV^{CTL} mice,
311 reaching statistical significance in the liver, thereby confirming enhanced hepatic insulin
312 signaling (Figure 4A). Additionally, we observed a general trend toward increased AMPK
313 (Thr172) phosphorylation across tissues, a pathway known to mediate adiponectin's effects
314 on lipid metabolism and energy homeostasis (Figure 4B). This effect was significant in skeletal
315 muscle, suggesting enhanced metabolic flexibility in this tissue (Figure 4B). We further
316 investigated plasma ceramide levels, given the ceramidase activity linked to AdipoR signaling
317 and the well-established lipotoxic role of ceramides in insulin resistance. Notably, $EV^{PP\text{-}Adpn}$
318 treatment significantly decreased total ceramides (Figure 4C), dihydroceramides (Figure 4D),
319 and hexosylceramides (Figure 4E), particularly long-chain subspecies (C22:00 to C24:00),
320 consistent with the systemic metabolic improvements observed. Altogether, these findings
321 support that $EV^{PP\text{-}Adpn}$ enhances tissue-specific insulin signaling via engagement of the
322 adiponectin pathway, in line with transcriptional data indicating restored insulin
323 responsiveness.
324
325

326 **Discussion**

327

328 Adpn is a promising target for managing T2D-related cardiometabolic complications by
329 enhancing insulin sensitivity, but the lack of stable, bioactive multimeric forms has so far
330 hampered its therapeutic development. To address this, we engineered two types of Adpn-
331 enriched EVs, either broadly distributed (EV^{Adpn}) or anchored at the surface ($EV^{PP\text{-}Adpn}$), using
332 a HEK-derived EV bioingeneering platform. Adoptive transfer of $EV^{PP\text{-}Adpn}$ in HFD-fed mice
333 improved insulin sensitivity, promoted insulin-driven adipose lipid storage, and reduced hepatic
334 steatosis, inflammation, and fibrosis. In contrast, EV^{Adpn} did not display such beneficial effects.
335 These results support the therapeutic potential of surface Adpn-enriched EVs as an innovative
336 strategy to counteract insulin resistance-related metabolic disorders such as T2D and
337 metabolic dysfunction-associated steatohepatitis (MASH).

338

339 In our study, mice injected intraperitoneally with increasing doses of control HEK293T-derived
340 EVs (EV^{CTL}, devoid of any Adpn) exhibited significant weight gain, especially at doses above
341 1.0×10^8 particles. Cross-study comparisons remain difficult due to variability in EV
342 quantification methods; NanoFCM, for example, tends to underestimate particle counts
343 compare to nanoparticle tracking analysis (NTA; SLL, *unpublished data*). Dosing strategies
344 also differ, with some studies relying on particle number and others on EV protein content.
345 Furthermore, most toxicity and immunogenicity assessments are performed under normal diet,
346 with limited evaluation of metabolic effects under HFD. Yet, the i.p. injection route and EV
347 origin (e.g., HEK293, allogeneic) may also influence immune responses, as HEK-derived EVs
348 can carry mildly immunogenic components[16,17]. Notably, the increase in neutrophils count post-
349 HEK293-derived EV injection may be relevant in HFD-induced obesity[17], given that obesity-
350 related inflammation involves neutrophil and macrophage recruitment in adipose tissue[18].
351 These observations stress the need to assess EV metabolic effects with proper controls
352 (vehicle, empty EVs) and under dietary stress conditions such as HFD, mimicking the
353 obesogenic nutritional environment.

354

355 $EV^{PP\text{-}Adpn}$, engineered to display Adpn specifically at the vesicle surface, exert significant
356 insulin-sensitizing effects, unlike EVs containing non-surface-anchored Adpn. This suggests
357 that surface-localized Adpn engages AdipoR1/R2 receptors, consistent with our previous
358 findings using lean adipose-derived EVs [6]. While no significant changes were observed in total
359 body weight or tissue mass, $EV^{PP\text{-}Adpn}$ improved insulin sensitivity, primarily in the liver, by
360 suppressing gluconeogenesis and reducing hepatic steatosis, inflammation, and fibrosis. In
361 adipose tissue, $EV^{PP\text{-}Adpn}$ induced insulin-regulated lipogenic and adipocyte remodeling genes,
362 promoting metabolically healthy expansion. These effects were accompanied by enhanced

363 glucose-stimulated insulin secretion, without altering pancreatic β-cell mass. In parallel, $EV^{PP-Adpn}$
364 reduced circulating ceramide levels, consistent with AdipoR-mediated ceramidase
365 activitation [19]. As ceramides are recognized as lipotoxic mediators impairing insulin signaling
366 and mitochondrial function, their reduction may drive the metabolic benefits observed, although
367 causality remains to be clarified [20]. Finally, the observed reduction in circulating FGF21 levels
368 following $EV^{PP-Adpn}$ treatment likely reflects a decreased need for compensatory hepatokine
369 secretion, consistent with restored hepatic metabolic function. This is relevant given that
370 elevated FGF21 levels in MASLD have been associated with impaired metabolic signaling and
371 FGF21 resistance, characterized by reduced receptor responsiveness despite high ligand
372 levels [15,21]. Its normalization may thus indicate a reversal of this dysfunctional axis and further
373 support the systemic metabolic benefits of $EV^{PP-Adpn}$.
374
375 Although $EV^{PP-Adpn}$ exert clear insulin-sensitizing effects, particularly in the liver and adipose
376 tissue, their capacity to reverse insulin resistance appears more modest than that observed
377 with native adipocyte-derived EVs [6]. This may reflect the combinatorial action of diverse
378 bioactive cargos within adipose EVs, including proteins, lipids, microRNAs or mitochondrial
379 components, acting synergistically to promote metabolic benefits [22]. Recent studies highlight
380 the beneficial effect of adipose cargos as engineering of EVs to enrich them with adipokines
381 reveal their beneficial metabolic potential. For instance, loading leptin into macrophage-derived
382 EVs thus successfully targeted the brain and restored breathing function in obese mice,
383 overcoming leptin resistance[23]. Similarly to our bioengineered Adpn EVs, apelin-loaded EVs
384 improved glucose tolerance and activated AMPK and Akt pathways in diabetic mice,
385 enhancing systemic insulin sensitivity [24]. In a separate study, EVs engineered for targeted
386 apelin delivery to pulmonary arterial hypertension lesions reversed pathological vascular
387 remodeling and improved cardiac function[25]. Finally, knowing that adiponectin is recognized
388 as one of the main downstream effectors of the metabolic effects of FGF21 on glucose
389 homeostasis and insulin sensitivity in mice [26], bioengineered EVs combining surface FGF21
390 and enclosed miR-223 demonstrated liver-preferential delivery and a marked reduction in the
391 MASH phenotype [27]. These examples underscore the therapeutic potential of combinatorial
392 EV cargoes in metabolic disease. Thus, while $EV^{PP-Adpn}$ already demonstrate insulin-sensitive
393 properties, their clinical optimization may require integration with complementary bioactive
394 payloads to fully recapitulate the potency of native adipose EVs.
395
396

397 **References**
398

399 1. Scherer, P.E., Williams, S., Fogliano, M., Baldini, G., and Lodish, H.F. (1995). A novel
400 serum protein similar to C1q, produced exclusively in adipocytes. J Biol Chem *270*,
401 26746-26749. 10.1074/jbc.270.45.26746.
402 2. Pajvani, U.B., Du, X., Combs, T.P., Berg, A.H., Rajala, M.W., Schulthess, T., Engel, J.,
403 Brownlee, M., and Scherer, P.E. (2003). Structure-function studies of the adipocyte-
404 secreted hormone Acrp30/adiponectin. Implications fpr metabolic regulation and
405 bioactivity. J Biol Chem *278*, 9073-9085. 10.1074/jbc.M207198200.
406 3. Straub, L.G., and Scherer, P.E. (2019). Metabolic Messengers: Adiponectin. Nat Metab
407 *1*, 334-339. 10.1038/s42255-019-0041-z.
408 4. Yamauchi, T., Kamon, J., Ito, Y., Tsuchida, A., Yokomizo, T., Kita, S., Sugiyama, T.,
409 Miyagishi, M., Hara, K., Tsunoda, M., et al. (2003). Cloning of adiponectin receptors
410 that mediate antidiabetic metabolic effects. Nature *423*, 762-769.
411 10.1038/nature01705.
412 5. Li, Y., Onodera, T., and Scherer, P.E. (2024). Adiponectin. Trends Endocrinol Metab *35*,
413 674-675. 10.1016/j.tem.2024.05.004.
414 6. Blandin, A., Amosse, J., Froger, J., Hilairet, G., Durcin, M., Fizanne, L., Ghesquiere, V.,
415 Prieur, X., Chaigneau, J., Vergori, L., et al. (2023). Extracellular vesicles are carriers of
416 adiponectin with insulin-sensitizing and anti-inflammatory properties. Cell reports *42*,
417 112866. 10.1016/j.celrep.2023.112866.
418 7. Cocozza, F., Grisard, E., Martin-Jaular, L., Mathieu, M., and Thery, C. (2020). SnapShot:
419 Extracellular Vesicles. Cell *182*, 262-262 e261. 10.1016/j.cell.2020.04.054.
420 8. Salomon, C., Das, S., Erdbrugger, U., Kalluri, R., Kiang Lim, S., Olefsky, J.M., Rice, G.E.,
421 Sahoo, S., Andy Tao, W., Vader, P., et al. (2022). Extracellular Vesicles and Their
422 Emerging Roles as Cellular Messengers in Endocrinology: An Endocrine Society
423 Scientific Statement. Endocr Rev *43*, 441-468. 10.1210/endrev/bnac009.
424 9. Claridge, B., Lozano, J., Poh, Q.H., and Greening, D.W. (2021). Development of
425 Extracellular Vesicle Therapeutics: Challenges, Considerations, and Opportunities.
426 Front Cell Dev Biol *9*, 734720. 10.3389/fcell.2021.734720.
427 10. Sotin, T., Ge, X., Schonke, M., Vince, L., Thouzeau, A., Frey, S., Lorant, V., Krul, L.,
428 Pronk, A.C.M., Lalai, R., et al. (2025). A rare gain of function variant of hepatic lipase
429 attenuates hypercholesterolemia and atherosclerosis in mice via an LDL receptor-
430 independent mechanism. Cardiovascular research. 10.1093/cvr/cvaf097.
431 11. Croyal, M., Kaabia, Z., Leon, L., Ramin-Mangata, S., Baty, T., Fall, F., Billon-Crossouard,
432 S., Aguesse, A., Hollstein, T., Sullivan, D.R., et al. (2018). Fenofibrate decreases plasma
433 ceramide in type 2 diabetes patients: A novel marker of CVD? Diabetes Metab *44*,
434 143-149. 10.1016/j.diabet.2017.04.003.
435 12. Mamoun, R., Trentin, B., and Polak, K. (2023). Chimeric adiponectin polypeptides,
436 extracellular vesicle comprising the same, and uses thereof. International patent
437 WO/2023/104822, patent application PCT/EP2022/084653 06.12.2022.
438 13. Samuel, V.T., and Shulman, G.I. (2016). The pathogenesis of insulin resistance:
439 integrating signaling pathways and substrate flux. J Clin Invest *126*, 12-22.
440 10.1172/JCI77812.
441 14. Rusli, F., Deelen, J., Andriyani, E., Boekschoten, M.V., Lute, C., van den Akker, E.B.,
442 Muller, M., Beekman, M., and Steegenga, W.T. (2016). Fibroblast growth factor 21
443 reflects liver fat accumulation and dysregulation of signalling pathways in the liver of
444 C57BL/6J mice. Scientific reports *6*, 30484. 10.1038/srep30484.

15. Fisher, F.M., Chui, P.C., Antonellis, P.J., Bina, H.A., Kharitonenkov, A., Flier, J.S., and Maratos-Flier, E. (2010). Obesity is a fibroblast growth factor 21 (FGF21)-resistant state. Diabetes *59*, 2781-2789. 10.2337/db10-0193.
16. Chen, Z.Q., Tang, T.T., Tang, R.N., Zhang, Y., Zhang, Y.L., Yang, H.B., Song, J., Yang, Q., Qin, S.F., Chen, F., et al. (2025). A comprehensive evaluation of stability and safety for HEK293F-derived extracellular vesicles as promising drug delivery vehicles. J Control Release *382*, 113673. 10.1016/j.jconrel.2025.113673.
17. Zhu, X., Badawi, M., Pomeroy, S., Sutaria, D.S., Xie, Z., Baek, A., Jiang, J., Elgamal, O.A., Mo, X., Perle, K., et al. (2017). Comprehensive toxicity and immunogenicity studies reveal minimal effects in mice following sustained dosing of extracellular vesicles derived from HEK293T cells. Journal of extracellular vesicles *6*, 1324730. 10.1080/20013078.2017.1324730.
18. Uribe-Querol, E., and Rosales, C. (2022). Neutrophils Actively Contribute to Obesity-Associated Inflammation and Pathological Complications. Cells *11*. 10.3390/cells11121883.
19. Holland, W.L., Miller, R.A., Wang, Z.V., Sun, K., Barth, B.M., Bui, H.H., Davis, K.E., Bikman, B.T., Halberg, N., Rutkowski, J.M., et al. (2011). Receptor-mediated activation of ceramidase activity initiates the pleiotropic actions of adiponectin. Nat Med *17*, 55-63. 10.1038/nm.2277.
20. Summers, S.A. (2018). Could Ceramides Become the New Cholesterol? Cell Metab *27*, 276-280. 10.1016/j.cmet.2017.12.003.
21. Geng, L., Lam, K.S.L., and Xu, A. (2020). The therapeutic potential of FGF21 in metabolic diseases: from bench to clinic. Nat Rev Endocrinol *16*, 654-667. 10.1038/s41574-020-0386-0.
22. Le Lay, S., and Scherer, P.E. (2025). Exploring adipose tissue-derived extracellular vesicles in inter-organ crosstalk: Implications for metabolic regulation and adipose tissue function. Cell reports *44*, 115732. 10.1016/j.celrep.2025.115732.
23. Freire, C., Ramsey, J.D., Pho, H., Kojima, R., Zhao, Y., Kim, L., Anokye-Danso, F., Berger, S., Ahima, R.S., Batrakova, E.V., et al. (2022). Leptin-loaded Extracellular Vesicles Treat Sleep-disordered Breathing in Mice with Obesity. Am J Respir Cell Mol Biol *67*, 720-723. 10.1165/rcmb.2022-0229LE.
24. Cui, J., Wang, M., Zhang, W., Sun, J., Zhang, Y., Zhao, L., Hong, Z., Li, D., Huang, Y.X., Zhang, N., and Chen, Y. (2024). Enhancing insulin sensitivity in type 2 diabetes mellitus using apelin-loaded small extracellular vesicles from Wharton's jelly-derived mesenchymal stem cells: a novel therapeutic approach. Diabetol Metab Syndr *16*, 84. 10.1186/s13098-024-01332-w.
25. Kim, J., Choi, Y.S., Kim, J., Wahab, R., Lee, Y., Joo, H., Park, S., Lee, I., Kim, S.A., Hwang, Y.H., et al. (2025). Targeted delivery of apelin using a novel extracellular vesicle platform for pulmonary arterial hypertension treatment. Biomaterials *323*, 123438. 10.1016/j.biomaterials.2025.123438.
26. Lin, Z., Tian, H., Lam, K.S., Lin, S., Hoo, R.C., Konishi, M., Itoh, N., Wang, Y., Bornstein, S.R., Xu, A., and Li, X. (2013). Adiponectin mediates the metabolic effects of FGF21 on glucose homeostasis and insulin sensitivity in mice. Cell Metab *17*, 779-789. 10.1016/j.cmet.2013.04.005.
27. Cho, H., Ju, H., Ahn, Y., Jang, J., Cho, J., Park, E., Kang, S.M., Lee, J., Seo, D., Baek, M.C., and Yea, K. (2025). Engineered extracellular vesicles with surface FGF21 and enclosed

miR-223 for treating metabolic dysfunction-associated steatohepatitis. Biomaterials *321*, 123321. 10.1016/j.biomaterials.2025.123321.

ACKNOWLEDGMENTS

We thank the SCAHU platform, especially Elodie Guillet, Jérôme Roux, Adeline Mourlan, Nina Meignan-Fizanne for mouse housing, care and technical assistance for animal functional exploration. We also thank the PACeM platform, especially L. Bonneau and J. Cayon, for qRT-PCR experiments.

The authors were supported the French National Research Agency (ANR-22-CE18-0026-02 EVADIPO). SLL is granted by Genavie, FHU GO NASH, Société Francophone du Diabète and the FFRD (sponsored by Fédération Française des Diabétiques, Abbott, AstraZeneca, Eli Lilly, Merck Sharp & Dohme, and Novo Nordisk).

The graphical abstract was created with BioRender.com

DECLARATION OF INTERESTS

These authors declare the following potential conflict of interests:

R.M. is a co-founder and CEO of Ciloa ; B.T is a co-founder and CSO of Ciloa.

B.T., K.P., and R.M. are inventors of patent WO2023104822A1 describing the stable anchoring of Adiponectin on EVs.

S.L.L. declare no competing interests.

All other authors declare no potential conflict of interest.

INCLUSION AND DIVERSITY

We support inclusive, diverse, and equitable conduct of research.

AUTHOR CONTRIBUTIONS

Methodology for EV production and characterization, A.B., M.L., K.P., R.M., B.T.

Methodology for animal experimentation and analysis, J.F., M.V., G.H., L.M., J.M., L.F., X.P., C.L.M., B.C., S.L.L.

Histology analysis, Q.M., J.C.

Blood biochemistry analysis, M.C.

Lipidomic analysis, M.C., M.G. ;

Conceptualization, S.L.L., B.C., R.M., B.T.

Writing – original draft, S.L.L.

Writing, review and editing, J.F., M.V., X.P., C.L.M., J.B., B.C., A.B., R.M.,S.L.L.

Supervision of the animal experimental part and project coordination, S.L.L.

All authors have read and agreed to the published version of the manuscript.

S.L.L. is the guarantor of this work and, as such, had full access to all the data in the study and takes responsibility for the integrity of the data and the accuracy of the data analysis.

Figure 1. Surface-anchored Adpn-EVs ($EV^{PP\text{-}Adpn}$) improve insulin sensitivity and glucose tolerance in HFD-fed mice.

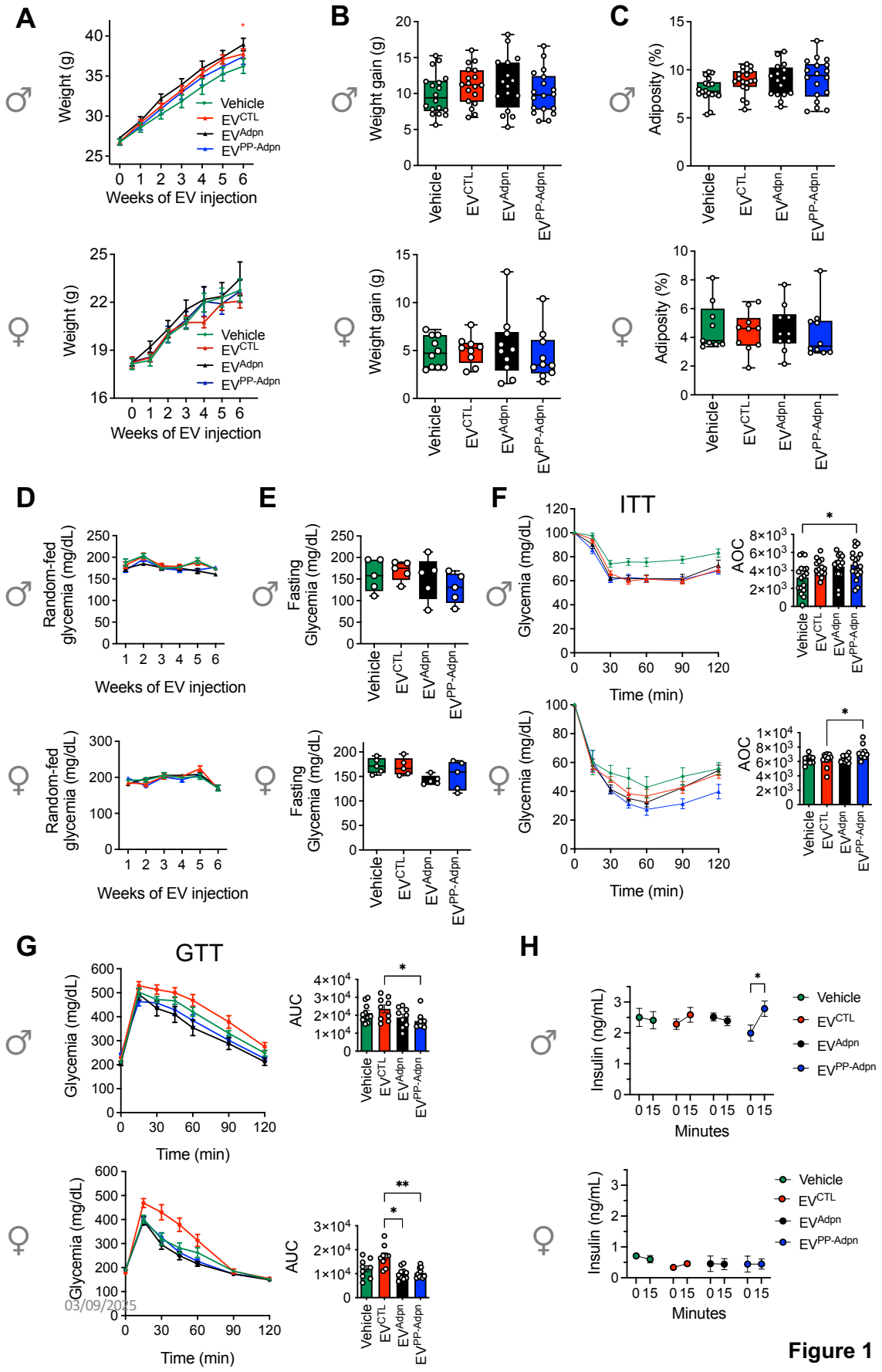

532

Figure 1

533

534 **Figure 1. Surface-anchored Adpn-EVs ($EV^{PP\text{-}Adpn}$) improve insulin sensitivity and**
535 **glucose tolerance in HFD-fed mice.**
536 **(A-C)** Body weight trajectory **(A)**, total weight gain **(B)**, and adiposity (%) at sacrifice **(C)** in
537 male (top) and female (bottom) HFD-fed mice after 6 weeks of i.p. injections with EV^{CTL}, EV^{Adpn}
538 or $EV^{PP\text{-}Adpn}$ (25 ng Adpn-equivalent per dose, or particle-matched EV^{CTL}) or vehicle (PBS).
539 **(D-E)** Random-fed glycemia measured throughout the experiment, n=16-18 for males (top);
540 n=9-10 for females (bottom) **(D)** and fasting glycemia measured at sacrifice **(E)** in males (top)
541 and females (bottom).
542 **(F)** Insulin tolerance tests (ITT) performed in males (top) and females (bottom), with area over
543 the curve (AOC) presented on the right.
544 **(G)** Intraperitoneal glucose tolerance tests (GTT) in males (top) and females (bottom), with
545 area under the curve (AUC) shown on the right.
546 **(H)** Insulin levels measured at baseline (T0) and 15 minutes post-glucose injection (T15) during
547 GTT in males (top) and females (bottom). Five animals per group were analyzed.
548 Data are presented as mean ± SEM. Dot plots represent the number of independent animals
549 analyzed. Statistical differences were calculated using one-way ANOVA followed a Tukey's
550 multiple comparisons test. *$p < 0.05$, **$p < 0.01$.

Figure 2. EV$^{PP\text{-}Adpn}$ promote promote insulin-sensitive AT expansion inducing healthy visceral adipose tissue remodeling

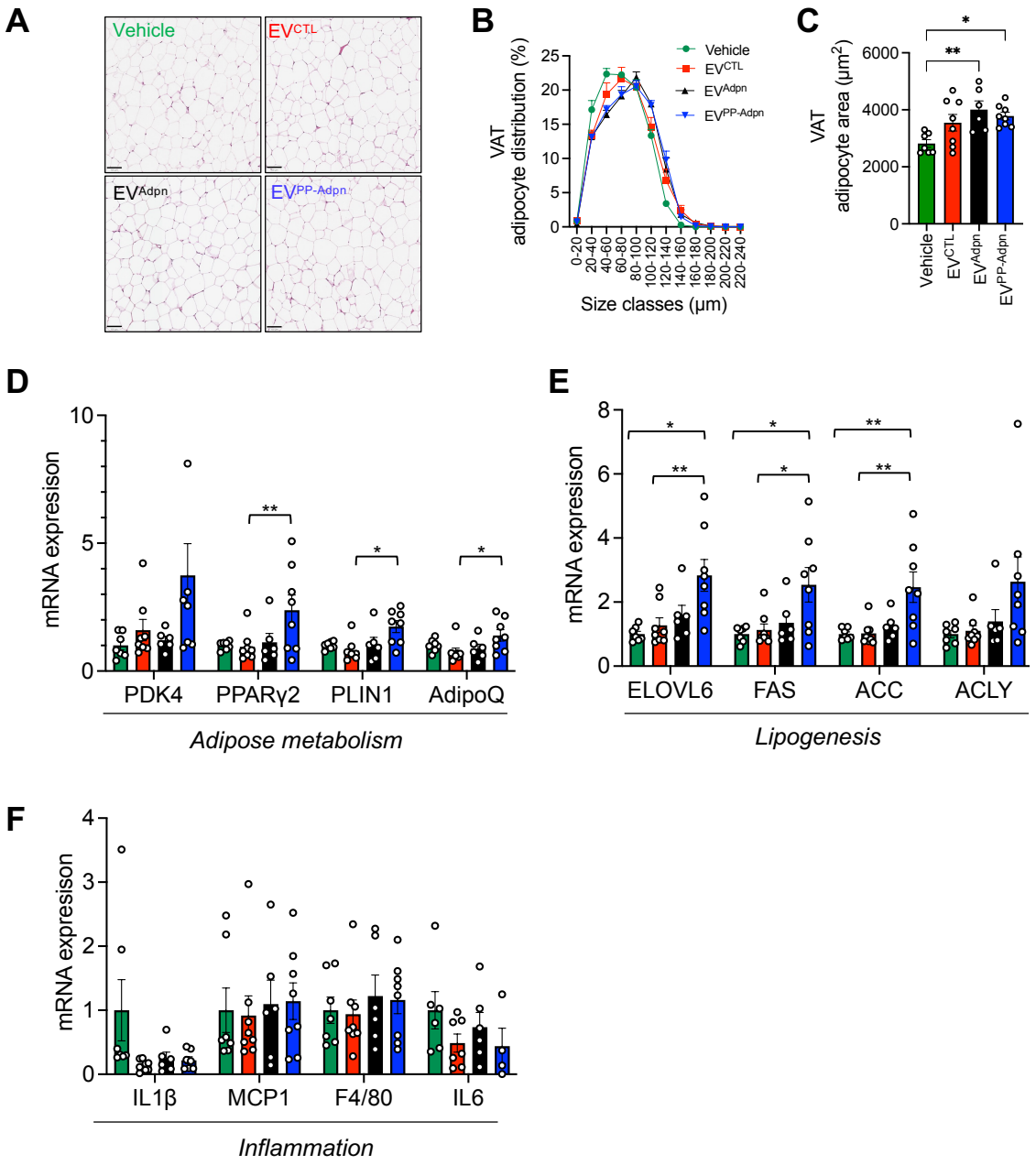

551

Figure 2

552 **Figure 2. $EV^{PP\text{-}Adpn}$ promote promote insulin-sensitive AT expansion inducing healthy**
553 **visceral adipose tissue remodeling**
554 **(A-C)** Histological analysis of VAT in male HFD-fed mice after 6 weeks of i.p. injections with
555 EV^{CTL}, EV^{Adpn}, or $EV^{PP\text{-}Adpn}$ (25 ng Adpn-equivalent per dose or particle-matched EV^{CTL}) or
556 vehicle (PBS). Representative hematoxylin–eosin (HE)-stained VAT sections are shown **(A)**,
557 from which adipocyte diameters were measured. Analysis of VAT adipocyte size distribution is
558 presented in **(B)**, and mean adipocyte area in **(C)**. n=6-8 animals per group were analyzed.
559 Scale bar, 100 µm.
560 **(D-F)** Quantitive PCR gene expression analysis in VAT from male HFD-fed injected mice.
561 mRNA expression was analyzed for key adipogenic markers (PDK4, PPARγ2, PLIN1, AdipoQ)
562 **(D)**, insulin-responsive lipogenic genes (ELOVL6, FAS, ACC, ACLY) **(E)** and pro-inflammatory
563 markers (IL1β, MCP1, F4/80, IL6) **(F)**. Bar colors: Green, Vehicle; Red, EV^{CTL}; Black, EV^{Adpn};
564 Blue, $EV^{PP\text{-}Adpn}$.
565 Data are presented as mean ± SEM. Dot plots represent the number of independent animals
566 analyzed. Statistical differences were calculated using one-way ANOVA followed a Tukey's
567 multiple comparisons test. *$p < 0.05$, **$p < 0.01$.

Figure 3. EV$^{PP\text{-}Adpn}$ reduce liver steatosis and improve MASLD/MASH-related gene expression signatures in HFD-fed mice.

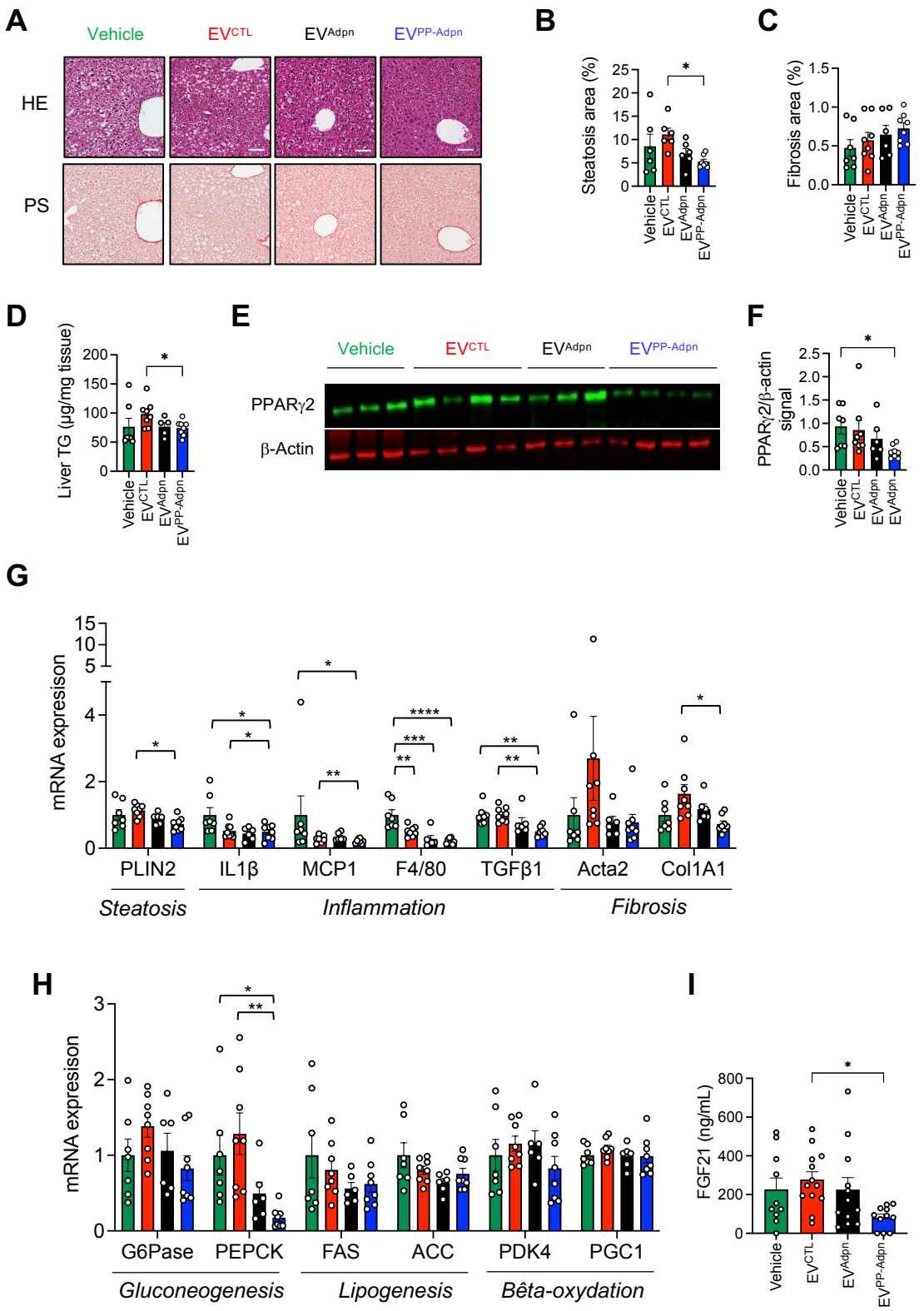

568

Figure 3

569 **Figure 3. $EV^{PP\text{-}Adpn}$ reduce liver steatosis and improve MASLD/MASH-related gene**
570 **expression signatures in HFD-fed mice.**
571 **(A-C)** Histological analysis of liver sections. Representative hematoxylin–eosin (HE) and
572 picrosirius red (PS) staining (A) are shown for male mice after 6 weeks of treatment with EV^{CTL},
573 EV^{Adpn} or $EV^{PP\text{-}Adpn}$ (25 ng Adpn-equivalent per dose, or particle-matched EV^{CTL}) or vehicle
574 (PBS). Quantification of steatosis area on HE-stained sections **(B)** and fibrosis area on PS-
575 stained sections **(C)** is presented. n=6-8 animals per group were analyzed. Scale bar, 100 µm.
576 **(D)** Biochemical measurement of hepatic triglyceride content.
577 **(E–F)** PPARγ2 protein expression in liver tissue from injected male mice. Representative
578 image blots **(E)** and protein quantification **(F)** are presented. β-actin serve as loading control.
579 **(G-H)** Quantitative PCR analysis of hepatic gene expression in HFD-fed injected male mice.
580 Relative mRNA levels of MASLD-associated genes **(G)** including steatotic (PLIN2), pro-
581 inflammatory (IL1β, MCP1, F4/80) and fibrotic markers (TGFβ1, Col1A1). Expression of key
582 metabolic genes **(H)** related to gluconeogenesis (PEPCK, G6Pase), lipogenesis (FAS, ACC)
583 and β-oxidation (PDK4, PGC1α). Bar colors: Green, Vehicle; Red, EV^{CTL}; Black, EV^{Adpn}; Blue,
584 $EV^{PP\text{-}Adpn}$.
585 **(I)** Circulating FGF-21 in injected male mice.
586 Data are presented as mean ± SEM. Dot plots represent the number of independent animals
587 analyzed. Statistical significance was assessed using one-way ANOVA followed by Tukey's
588 multiple comparisons test. *$p < 0.05$, **$p < 0.01$, ***$p < 0.001$, ****$p < 0.0001$.
589

Figure 4. EVPP-Adpn promote adiponectin-dependent insulin signaling and reduces plasma ceramide levels.

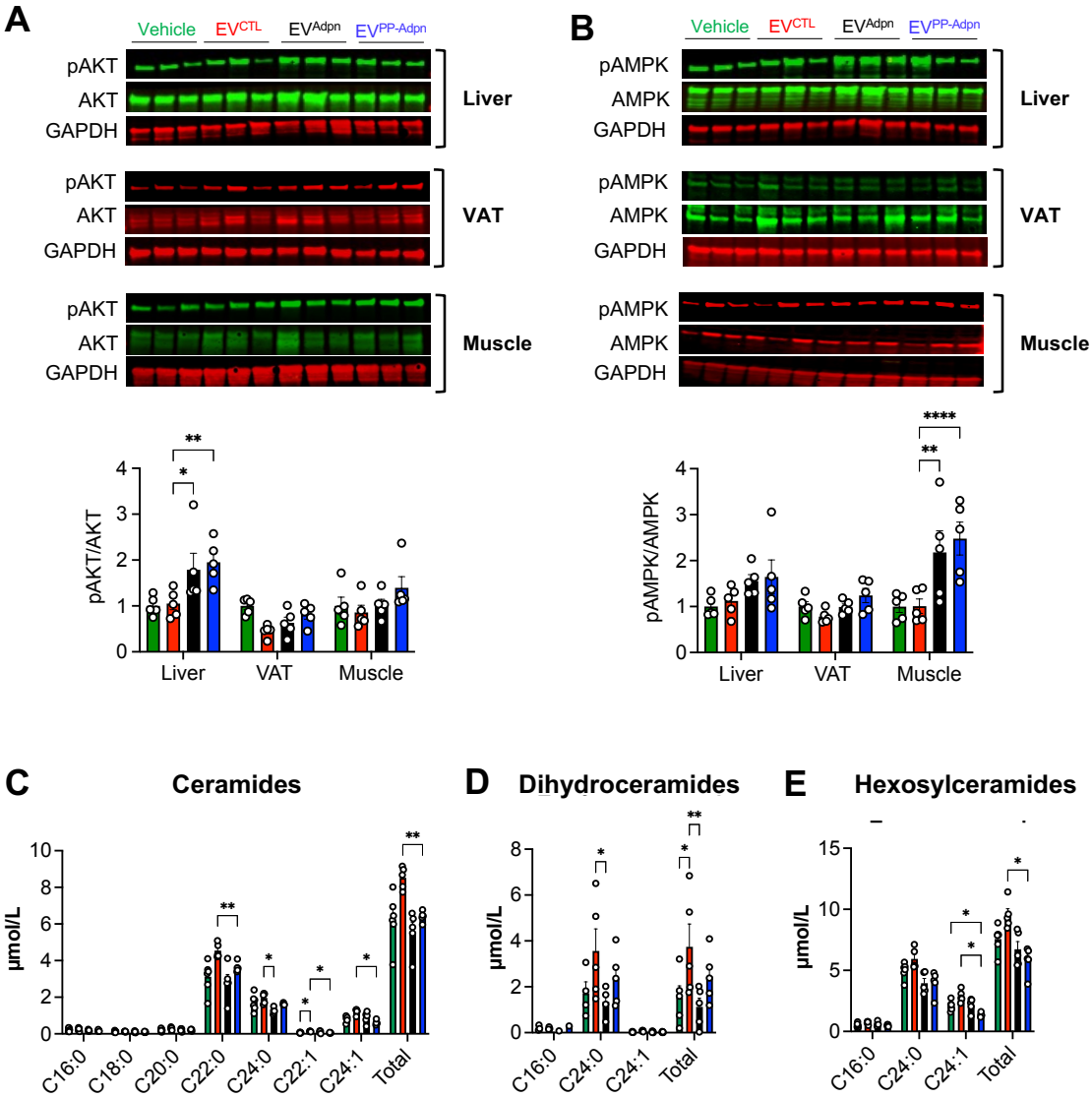

590

Figure 4

591 **Figure 4. $EV^{PP\text{-}Adpn}$ promote adiponectin-dependent insulin signaling and reduces**
592 **plasma ceramide levels.**
593 **(A-B)** Western blot analysis of AKT (Ser473) **(A)** and AMPK (Thr172) **(B)** phosphorylation in
594 liver, VAT, and skeletal muscle following insulin injection in mice. Representative blots are
595 shown, with GAPDH as loading control. Quantification of phospho-AKT/total AKT **(A)** and
596 phospho-AMPK/total AMPK ratios **(B)** are presented below the respective blots.
597 **(C-E)** Plasma ceramide profiling for total and subspecies of ceramides **(C)**, dihydroceramides
598 **(D)** and hexosylceramides **(E)**.
599 Data are presented as mean ± SEM. Dot plots represent the number of independent animals
600 analyzed. Statistical significance was assessed by one-way ANOVA with Tukey's post hoc
601 test. *$p < 0.05$, **$p < 0.01$, ****$p < 0.0001$.